Bioactive Materials 27 (2023) 461–473

Contents lists available at ScienceDirect

Bioactive Materials

journal homepage: www.keaipublishing.com/en/journals/bioactive-materials

Multifunctional two-component in-situ hydrogel for esophageal submucosal dissection for mucosa uplift, postoperative wound closure and rapid healing

Xiong-Xin Lei [a,1], Juan-Juan Hu [a,b,1], Chen-Yu Zou [a], Yan-Lin Jiang [a], Long-Mei Zhao [a], Xiu-Zhen Zhang [a], Ya-Xing Li [a], An-Ni Peng [c], Yu-Ting Song [a], Li-Ping Huang [a], Jesse Li-Ling [a,d], Hui-Qi Xie [a,*]

[a] Department of Orthopedic Surgery and Orthopedic Research Institute, Laboratory of Stem Cell and Tissue Engineering, State Key Laboratory of Biotherapy, West China Hospital, Sichuan University, Chengdu, Sichuan, 610041, China
[b] Department of Otolaryngology, Head and Neck Surgery, West China Hospital, Sichuan University, Chengdu, Sichuan, 610041, China
[c] Institute of Biomedical Engineering and Informatics, Ilmenau University of Technology, Gustav-Kirchh Off Str. 2, 98693, Ilmenau, Germany
[d] Department of Medical Genetics, West China Second Hospital, Sichuan University, Chengdu, Sichuan, 610041, China

ARTICLE INFO

Keywords:
Hydrogel
Endoscopic submucosal dissection
Mucosa uplift
Tissue sealant
Wound healing

ABSTRACT

Endoscopic submucosal dissection (ESD) for gastrointestinal tumors and premalignant lesions needs submucosal fluid cushion (SFC) for mucosal uplift before dissection, and wound care including wound closure and rapid healing postoperatively. Current SFC materials as well as materials and/or methods for post-ESD wound care have single treatment effect and hold corresponding drawbacks, such as easy dispersion, short duration, weak hemostasis and insufficient repair function. Thus, designing materials that can serve as both SFC materials and wound care is highly desired, and remains a challenge. Herein, we report a two-component *in-situ* hydrogel prepared from maleimide-based oxidized sodium alginate and sulfhydryl carboxymethyl-chitosan, which gelated mainly based on "click" chemistry and Schiff base reaction. The hydrogels showed short gelation time, outstanding tissue adhesion, favorable hemostatic properties, and good biocompatibility. A rat subcutaneous ultrasound model confirmed the ability of suitable mucosal uplift height and durable maintenance time of AM solution. The *in vivo/in vitro* rabbit liver hemorrhage model demonstrated the effects of hydrogel in rapid hemostasis and prevention of delayed bleeding. The canine esophageal ESD model corroborated that the *in-situ* hydrogel provided good mucosal uplift and wound closure effects, and significantly accelerated wound healing with accelerating re-epithelization and ECM remodeling post-ESD. The two-component *in-situ* hydrogels exhibited great potential in gastrointestinal tract ESD.

1. Introduction

Endoscopic submucosal dissection (ESD) is a commonly used minimally invasive technique for removing premalignant lesions and early tumors of the gastrointestinal (GI) tract [1,2]. However, thermal injury procedure by ESD can lead to intra- and/or postoperative complications such as bleeding, perforation, infection and stricture [3–5], which may seriously affect the quality of life of patients. Therefore, the SFC materials, as a buffer layer between the mucosa and muscle layers pre-operation, are introduced to reduce above complications [6]. Current SFC materials, including hypertonic saline, hypertonic glucose, glycerol fructose, sodium hyaluronate, succinyl gelatin and fibrinogen etc. [7], have limited use due to their short duration, poor injectability, and safety concerns [8,9]. Thus, long-acting uplifting fluid is the

Abbreviations: ESD, Endoscopic submucosal dissection; SFC, Submucosal fluid cushion; GI, Gastrointestinal; SA, Sodium alginate; ADA, Oxidized sodium alginate; CMCS, Carboxymethyl chitosan; AM, Maleimide-based oxidized sodium alginate; CS, Sulfhydryl carboxymethyl chitosan.

Peer review under responsibility of KeAi Communications Co., Ltd.

* Corresponding author.
E-mail address: xiehuiqi@scu.edu.cn (H.-Q. Xie).

[1] These authors have contributed equally to this work.

https://doi.org/10.1016/j.bioactmat.2023.04.015
Received 12 February 2023; Received in revised form 29 March 2023; Accepted 16 April 2023

uppermost strategy to maintain an appropriate height of the uplift mucosa [2], which can help to minimize the surgical procedure and prevent complications such as intraoperative bleeding and perforation [3,10]. Besides, wound closure after ESD is another strategy proposed to enhance hemostasis, prevent infection and accelerate wound healing [11–13]. To achieve this, thermal coagulation, mechanical methods (hemostatic clips, ligatures, etc.) as well as drugs and materials have been introduced for post-ESD wound closure [14–17]. However, due to various shortcomings, e.g., mismatched cover degradation with ulcer healing, limited ulcer healing-promoting effect, and even serious side effects (delayed perforation, severe infection etc.), above methods have not been applied for routine clinical use [18]. Moreover, to adapt to the strong peristaltic nature and complex physiology of the gastrointestinal tract, the properties of outstanding durability and convenient delivery for materials are also required. Despite considerable research progress has been made in post-operative wound care, insufficient durability *in situ* (e.g., fibrin glue, etc.) [19] and inconvenient delivery (e.g., hemostatic sprays, porous gelatin membranes, etc.) of the materials or drugs is still unaddressed [13,20]. Thus, materials with multifunctional such as mucosa uplift, wound closure, ease of delivery and proper tissue adhesion would be a desirable alternative and might achieve an optimal outcome for ESD.

Hydrogels are tissue-like polymers with high water content, low modulus and diffusivity, and have a great potential to be applied as the SFC materials for extended uplifting time [21]. Yet conventional hydrogels cross-linked by chemical bonds or physical interactions are usually unsuitable for injection through endoscopic needles [22]. Physically cross-linked hydrogels, e.g., thermally triggered gelation, may also encounter the same problem during injection [23]. Fortunately, *in situ-formed* injectable hydrogels (ISFIHs) may provide an effective solution to above dilemma [21]. Specifically, the ISFIH is initially a liquid at room temperature and has a pre-gelling fluidity that can be applied to any defect or cavity with minimal invasiveness [24–26]. ISFIHs could be formed *in situ* and can rapidly cross-link with the tissues around the wound site to act as a bio-adhesive material to bind tissues together, sealing wounds and stopping unwanted bleeding [26–30]. The hysteretic gel formation and tissue adhesion characteristics of *in situ* hydrogels offer the possibility to address both intraoperative mucosal-uplifting and postoperative wound-closuring of the ESD. However, until now, there have been no reports on any type of hydrogel that can simultaneously address mucosal dissection and postoperative care and can be used in clinical ESD.

We hereby describe a multifunctional two-component *in-situ* hydrogel for esophageal ESD. Two natural biomolecules, sodium alginate (SA) and carboxymethyl chitosan (CMCS), which have several excellent biological properties and are widely used in biomedical applications [31–34], were modified into two derivatives, maleimide-based oxidized sodium alginate ADA-Mal (abbr. to AM) and sulfhydryl carboxymethyl chitosan CMCS-SH (abbr. to CS). Of the two derivatives, the AM component can serve as the SFC material for its high viscosity, while the CS solution with a lower viscosity can be sprayed onto the wound after mucosal dissection. The two solutions are able to cross-link rapidly to form a gel based on the reaction principles of "click chemistry" and Schiff base upon contact with the wound surface. The viscosity of AM solution and durable uplift height as well as lasting time of the subcutaneous cushion as the SFC material was determined by viscosity detection and subcutaneous ultrasonic detection in rats. Among them, the AM7 (7 wt %) solution showed a better uplifting effect, and the effect was further confirmed in the canine esophageal model. The tissue adhesion and wound closure ability of *in-situ* hydrogel were investigated by bursting test and rabbit liver hemostasis test *in vitro/in vivo*, respectively. Finally, the function of mucosal uplift, wound hemostasis, sealing and promoting healing of the *in-situ* hydrogel were verified in the canine esophageal ESD model, and the effect was consistent with the *in vivo* experiment. All in all, a multifunctional two-component *in-situ* hydrogel with individualized characteristics for gastrointestinal tract ESD was prepared in this study, and the chemical structure, rheology, gel-forming time, morphology, swelling behavior, adhesiveness, *in vitro/in vivo* biocompatibility, mucosal uplifting effect, hemostasis, wound sealing and therapeutic efficacy were systematically characterized. All of the results suggested that the *in-situ* hydrogels wound dressings exhibit great clinical potential for GI tract ESD treatment. Fig. 1 shows the schematic diagram of the material modification, hydrogel preparation and application process in the canine esophageal ESD in this study.

2. Results and discussion

2.1. Synthesis and characterization of the multifunctional Hydrogel

2.1.1. Characterization of the synthetic materials

Two biological macromolecules, SA and CMCS, were modified and grafted following the path diagram shown in Fig. 1, S1a and S1b to obtain two derivatives, maleimide-based oxidized alginate (AM) and sulfhydryl carboxymethyl chitosan (CS), respectively. The derivatives were characterized via FTIR and ^{1}H NMR. Details of FTIR and ^{1}H NMR spectra of SA, CMCS and their derivatives are shown in Figs. S1c and S1d in the Supplementary. The oxidation degree of sodium alginate oxide (ADA) was measured by the hydroxylamine hydrochloride method, and the oxidation-degree was 47.5 ± 2.69%. The FTIR and ^{1}H NMR spectra showed that the maleimide group (-Mal) and the sulfhydryl group (-SH) were successfully grafted onto ADA and CMCS, respectively. The degree of substitution (DS) of the maleimide groups in AM and the sulfhydryl groups in CS were about 27.29% and 48.2%, respectively.

2.1.2. Hydrogel synthesis and gelation mechanism

The gels of A*x*C*y* (*x, y* = 3, 4, 5, 6, 7) (In the A*x*C*y* formula, A*x* and C*y* are abbreviations for AM*x* and CS*y*, respectively, and *x, y* = 3, 4, 5, 6, 7 represent the mass percentages of 3 wt%, 4 wt%, 5 wt%, 6 wt% and 7 wt % of AM or CS, respectively) were obtained by mixing equal volume of AM and CS (Fig. 2a–c). Multiple molecular bonds attribute to the formation of the hydrogels. The –SH groups in the CS can form a stable thioether bond with the -Mal groups in the AM through Michael addition reaction, which occurs within a few seconds. The aldehyde groups in the ADA can form imide bonds with the primary amine groups (-NH_2) in the CS. In addition, $Na_2B_4O_7$ (borax) in the CS solution can decompose into $B(OH)^{4-}$ and $B(OH)_3$, and the alkaline environment accelerates the Michael addition reaction. Meanwhile, -S^- decomposed from –SH can also react with each other to form disulfide bonds (-S-S-). Moreover, borate-diol bonds between alcohol hydroxyl groups in polysaccharides and $B(OH)^{4-}$ can also accelerate the gelation [35,36]. The multiple cross-linking strengthens the interpenetrating network inside the hydrogel (Fig. 1), leading to stable gel formation (Fig. 2d). The color of the hydrogel deepens with the increasing of AM (Fig. 2e(i), (ii) and (iii)), which may be attributed to the imide bond (-C═N-) formed by the Schiff base reaction occurring, and deepened with the number of groups [37, 38]. Moreover, the color degree of the gel is also influenced by the gelation rate. The Michael addition reaction between -Mal and –SH is the rate-limiting step in gel formation, which occurs immediately upon the two groups contact. Both AM7 and CS7 are rich in -Mal and –SH groups, respectively, and can gel rapidly at the interface where the two solutions come into contact, thus preventing further contact of the two solutions and reducing the formation of more imide bonds; therefore, it can be seen that the A7C3 gel presents a darker brown color than the A7C7 gel (Fig. 2e (iv)).

2.1.3. Gelling time of the hydrogels

Suitable gelling time is necessary for shortening the operative time and emergency treatment for severe bleeding scenes. Specifically, the gelling time of the gel was measured by the stirring-inversion method (Video 1). The gelling time is about 3–10 s of A*x*C*y* (*x, y* = 3, 4, 5, 6, 7) hydrogel (Fig. 2e), which depends on the degree of Michael addition reactions occurring in the AM and CS solutions. Among them, the gelling

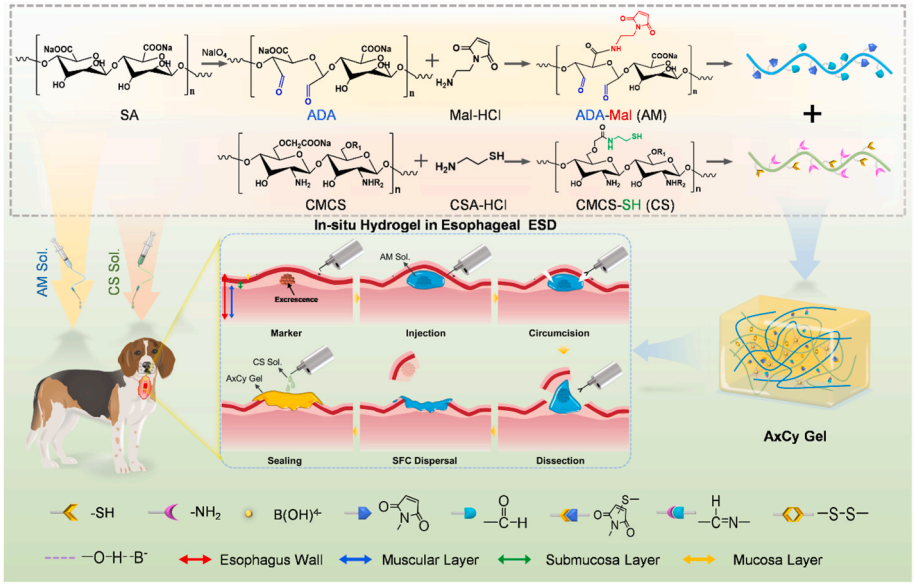

Fig. 1. Schematic diagram showing the design principle of multifunctional hydrogel and its application in canine esophageal ESD.

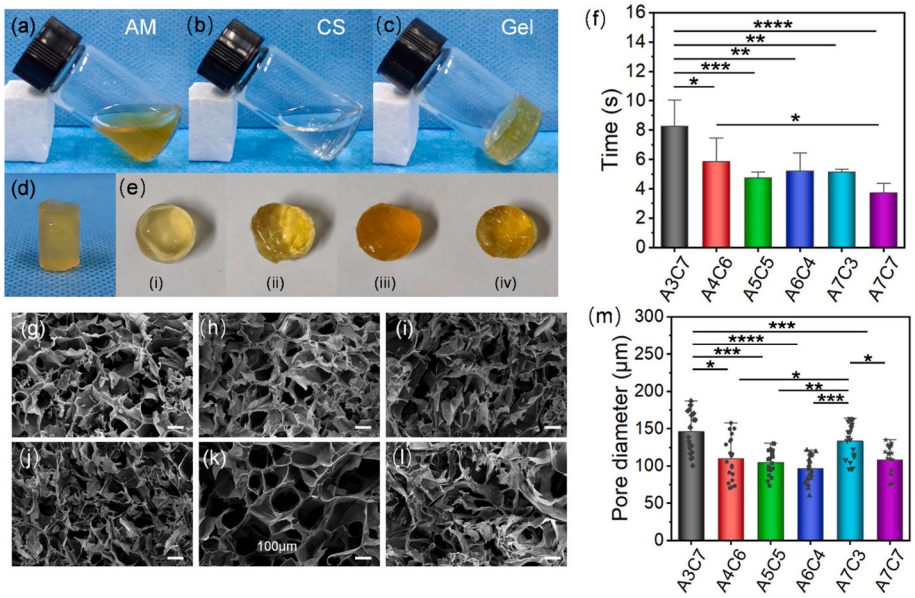

Fig. 2. Morphology and physicochemical properties of the hydrogels composed of AM and CS. (a) AM solution. (b) CS solution. (c) A*x*C*y* (*x*, *y* = 3, 4, 5, 6, 7) hydrogels. (d) Columnar morphology of the hydrogels after stabilization. (e) Morphology of the hydrogels with different components: (i) The A3C7 hydrogel, (ii) The A5C5 hydrogel, (iii) The A7C3 hydrogel, (iv) The A7C7 hydrogel. (f) Gel formation time of the hydrogels. (g–l) SEM images of A3C7, A4C6, A5C5, A6C4, A7C3, A7C7 hydrogel lyophilized scaffolds, respectively, at 50 × . (m) Internal pore size statistics of hydrogel lyophilized scaffolds. (*$P < 0.05$, **$P < 0.01$, ***$P < 0.001$, ****$P < 0.0001$, and n = 3).

time of the A3C7 gel is the longest, and that of the A7C7 gel is the shortest, with an average of 8.3 ± 1.5 s and 3.7 ± 0.56 s, respectively, which is an appropriate operation time for gastrointestinal tract ESD.

Supplementary video related to this article can be found at https://doi.org/10.1016/j.bioactmat.2023.04.015

2.1.4. Internal structure of the hydrogels

From the SEM results, the internal pore structure of the hydrogel presents lamellar or honeycomb interlaced arrangement (Fig. 2g–l). The average internal pore sizes in the A3C7 (146.3 ± 28.17 μm) and A7C3 groups (133.7 ± 24.91 μm) were significantly larger than that of the other groups (Fig. 2m). Analysis of the internal pore size distribution of the scaffold showed that when the ratio of AM and CS groups was larger (> 100%), the internal structure was sparser and the pore size was greater. We inferred that the internal pore size of the hydrogels depends on the intermolecular network structure, and the greater the intermolecular force inside the hydrogel, the denser intermolecular network will be formed, resulting in a more regular pore-like structure.

2.1.5. Rheological behavior of the hydrogels

To describe the effect of different ratios of AM and CS solutions on the rheological behavior of hydrogels. The rheological properties of the A*x*C*y* (*x*, *y* = 3, 4, 5, 6, 7) hydrogels were investigated using a modular intelligent advanced rotary rheometer (Anton Paar GmbH, MCR302, Austria) (Fig. S2a). From the rheological curve, when in the shear amplitude-sweep mode was performed at a frequency of 1 Hz, and conducted at a strain of <10%, the hydrogel behaves as an elastic solid in all groups (G' > G″) (Fig. S2b). The G′ value of each group was recorded (Fig. S2d); when strain >100%, the gels were crashed (G' < G″).When the oscillatory frequency sweep was conducted at a strain of <10%, the hydrogels were stable and behave as elastic solids at the frequency between 0.1–10 Hz (G' > G″) (Fig. S2c); the G′ values of groups A3C7, A4C6, A5C5, A6C4, A7C3, A7C7 were recorded, and increased in order from the rheological curve and statistics, among

which G′ value of groups A5C5 and A6C4 were similar (Fig. S2e). The rheological behavior of the hydrogels was consistent in both sweep modes.

2.1.6. Swelling properties of the hydrogels

Swelling is one of the most important properties of hydrogels, which is important for the transport of nutrients, oxygen and water exchange [39]. The swelling properties of the hydrogels were evaluated by immersing in PBS buffer till swelling to equilibrium. From the swelling curve, the hydrogels swelled to equilibrium in the PBS buffer after about 30 h (Fig. S2f). The swelling rate of the A7C3 gel (101.9 ± 14.63%) and A3C7 gel (94.34 ± 10.75%) is greater than that of A7C7 gel (55.77 ± 6.39%). The dissolution rate of hydrogel showed a trend of increasing and then decreasing, in which the degradation started after 30h.

Taken together, we concluded that the morphology, rheological behavior, swelling properties of the hydrogels are probably related to the bond types within the hydrogel. From the study, the Michael addition reaction determines the rate of gel formation, and the degree of reaction proceeds is related to the amount of maleimide and sulfhydryl groups as well as the viscosity effect of the solution [40]. Specifically, the lower the viscosity, the better contact between the two reaction solutions. Adequate contact of reactive groups (e.g. $–NH_2$, –SH, –COH, –C═C-, $B(OH)^{4-}$, –OH, etc.) in the reaction solution can form a denser cross-linked network, thus leading to better mechanical properties. There is no doubt about that the viscosity of the AM and CS solutions increased with increasing mass percentage, and the viscosity of AM solution was much higher than that of CS solution at the same percentage content (Fig. 5a and b). Compared to the A7C7 gel, the A7C3 gel exhibited larger internal pore size and swelling rate, which may be attributed to more thorough reaction and more stable internal network structures. The difference in bonding types between gels may be the main reasons for the difference in performance. The Schiff base reaction, which is widespread in A3C7 gels, has a low reaction rate and can continually form reversible imide bonds after the Michael addition reaction, allowing the gels to withstand greater deformation. Moreover, the interactions between hydrogen bonds and reactive groups (-OH, $–NH_2$, –COH and –CONH, etc.) also affect the mechanical properties of the gels [41]. In conclusion, the cross-linked network inside the A*x*C*y* (*x, y* = 3, 4, 5, 6, 7) hydrogel is the result of multiple intermolecular forces, and it is difficult to tell the individual contribution of the bonds to the multiple physical properties of the hydrogel. The A7C3 gel combination exhibits appropriate physical properties (gelation time, pore size, swelling properties) and a suitable one-component viscosity for submucosal injection and postoperative wound closure, making it the preferred choice for follow-up studies.

2.2. Adhesive properties of the Hydrogel

2.2.1. Tissue adhesion

Compared with the traditional hemostatic method, the hemostatic mechanism of hydrogels mainly relies on the good tissue adhesiveness that can adhere to wound sites with a short gelation time. Specifically, the adhesion layer formed by the gel on the wound site acts as a physical barrier to seal the wound and prevent blood outflow [42]. In addition, the GI tract is an open and complex environment, and post-ESD wounds are often irregularly shaped and require certain tension; therefore, as a material for post-ESD closure in GI tract, hydrogel not only needs to be able to adapt to the irregular wound shape post-operative and resist the continuous peristalsis of the GI tract as well as the pH fluctuations in different sites, but also needs to have certain self-healing ability. The pH of the GI tract is known to vary widely from highly acidic (pH 1–3) in the stomach to neutral or weakly alkaline in the duodenum, jejunum and ileum (pH 6–7.5) [43,44]. Thus, the adhesion behavior, shear strength, rheological behavior and compressive strength of the *in-situ* hydrogel were investigated by performing porcine skin adhesion test, lap-shear test, self-healing ability test, and bursting test, respectively.

The tissue adhesion of the hydrogels was evaluated by the adhesion of the hydrogels to porcine skin. Specifically, the hydrogel was formed *in situ* on a piece of porcine skin with the surface grease removed, and after the gelling was stabilized, forces of different orientations (stretch, bend, extrude, twist) were applied to the skin to observe the adhesion of the hydrogel to the skin (Fig. 3a). From the results, the gel on the porcine skin can still adhere firmly to the porcine skin even after experiencing repeated anisotropic forces, showing good tissue adhesion. The GI tract is an environment with a wide range of pH (1–7.5). To verify the stability and tissue adhesion of hydrogels in different pH environments, the porcine skin adhered with hydrogels was immersed in dilute hydrochloric acid solution (pH = 1.2) and PBS solution (pH = 7.4), respectively (Fig. 3b). To better simulate the adhesion of hydrogels in the scenarios of peristalsis in GI tract, the gel-adhered-skin immersed in different pH solutions were allowed to undergo vibration at 60 rpm/min, and after 72 h, as before, forces of anisotropic were applied to the skin to observe the adhesion of hydrogels to porcine skin. As shown in Fig. 3b, the gel on the skin surface of both groups remained firmly adhered and did not peel off under experimental conditions. However, the surface of the gel in the PBS group was partially broken and exfoliated after 72 h of immersion. The gel's morphology in the HCl group has remained intact, while the volume decreased compared to the initial state, which may be due to mechanical force disruption caused by shaker vibration and degradation.

Surgical wounds are often irregular shape, and a good tissue adhesive should be able to accommodate irregular wounds of any shape. The adhesion of hydrogel to irregular wounds was simulated by *in-situ* gelling in a "☆" shaped groove etched on the porcine skin surface. Once the gel has formed and stabilized, the interface between the gel and the attached tissue was flushed with running water to observe the gel shedding. As shown in Fig. 3c, the gel remained firmly adhered to the wound and did not peel off when rinsed with a washing bottle. Lap-shear tests were carried out to evaluate the tissue adhesion properties of the hydrogels (Fig. S3a). As shown, the A7C3 gel has attained good tissue adhesion, with a strength greater than that of Fibrin glue (Figs. S3b and 3c). The self-healing ability of the hydrogel was tested by a rheometer in the alternating step-strain sweep mode. As shown in Fig. S4, the hydrogel structure was destroyed at a strain of 300% (G' < G″) and restored at a strain of 1% (G' > G″). When the oscillatory strain has switched back and forth between 1% and 300%, the hydrogel also switched between reconstruction and destruction, showing a good self-healing ability.

The adhesion tests have illustrated that the hydrogels prepared could attain good tissue adhesion and can adapt to the variable pH environment of the GI tract as well as irregular wounds. More importantly, the hydrogel can continue to act on the wound closure by self-healing even if it is disrupted by creeping or moving tensions.

2.2.2. Burst strength of the hydrogels

As we know, blood pressure will be produced in the process of bleeding, while hemostatic material should have certain resistance to rupture strength. The ability of hydrogels to resist blood pressure as wound sealants was verified by bursting test. The experimental setup is shown in Fig. 3d. Specifically, a porcine skin with a hollow "1"-shaped hole was fixed above the chamber of a bursting experimental device, and after the gel was formed and stabilized *in situ* in the "1"-shaped hole, water was slowly injected into the chamber through a syringe attached to one end of the tee tube until the hydrogel was completely broken by water pressure. The maximum breaking pressure was recorded by a pressure gauge connected to the other end of the tee tube. Commercial fibrin glue for clinical use was used as a control. The working schematic of the device is shown in Fig. 3e. The test results showed that the maximum bursting pressure of A7C3 gel and fibrin glue were 9.51 ± 1.20 kPa and 10.16 ± 0.78 kPa (Fig. 3f), respectively, showing no significant difference.

The *in-situ* hydrogels exert tissue adhesion may be attributed to the

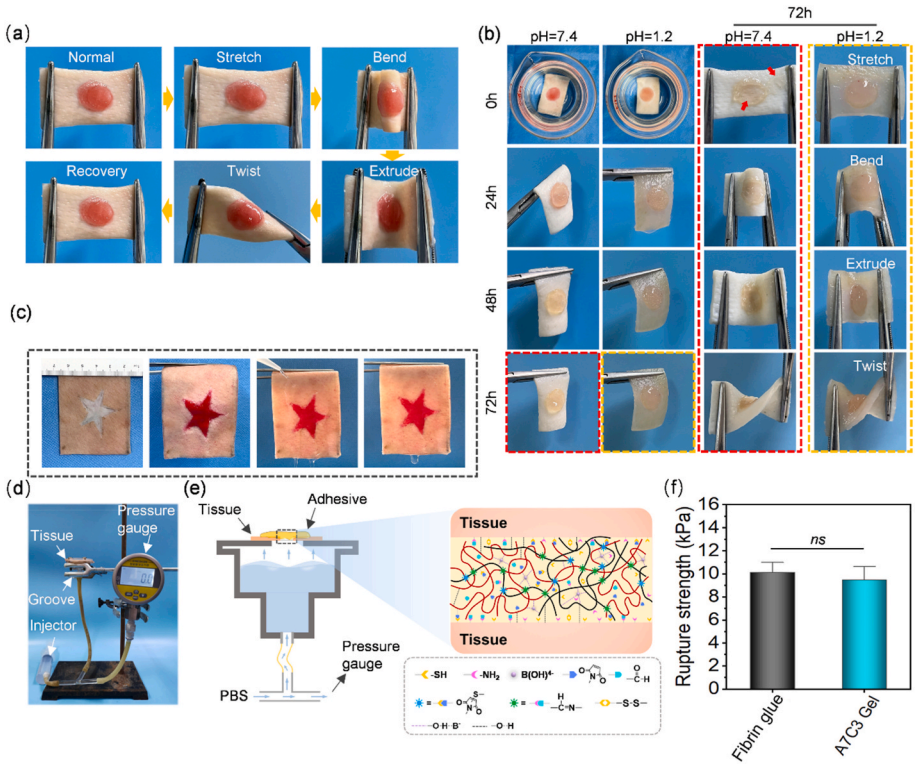

Fig. 3. *In vitro* assessment of the tissue adhesion of the hydrogels. (a) A7C3 hydrogel gelation *in situ* on the porcine skin surface followed by applying of force in various orientations (e.g., stretching, bending, extruding, twisting). (b) Effect of different pH solutions (pH = 1.2 and 7.4) on hydrogel adhesion. (c) The gel is formed *in situ* in the groove of the porcine skin with a "☆" shape, followed by rinsing the boundary between the gel and tissue adhesion with running water to simulate the adhesion behavior of the hydrogel in irregular wounds. (d) Diagram of the test device for the bursting test. (e) Schematic diagram of the bursting test, and the principle of adhesion between the hydrogels and tissues. (f) Average rupture pressure of commercially available fibrin glue and the A7C3 hydrogel (n = 3). (*ns*: no significant difference).

reaction of the active groups in the gel with that of tissue surface. Two types of reactions may occur when the gel exerts tissue adhesion. One is the Schiff base reaction between the free aldehyde group in AM and the ε-amino group of the lysine or hydroxylysine in the tissue [37,45], another is the Michael addition reaction between the maleimide group in AM and cysteine sulfhydryl groups in mucins [7]. In addition, the free sulfhydryl groups in the hydrogel can form disulfide bonds with sulfhydryl groups in cysteine in the tissue. Groups such as –OH, $–NH_2$, and –CONH– in the hydrogel can also form hydrogen bonds with tissue surface groups (e.g., –OH and $–NH_2$), which may further strengthen the interfacial bonding between the gel and the tissue (Fig. 3e) [41]. Adhesion tests and bursting test have showed that the adhesion of *in-situ* hydrogels to tissues is based on chemical binding reactions between groups rather than physical adsorption. Moreover, as a tissue adhesive/sealant, the hydrogel has certain burst resistance strength, which have potential application in wound closure and hemostasis.

2.3. Biocompatibility of the Hydrogel

A prerequisite for hydrogels used as tissue sealant applications is good biocompatibility, which includes cytocompatibility, hemocompatibility, and histocompatibility. NIH-3T3 cells was used for evaluating the cytocompatibility of the hydrogels. The cells were co-cultured with the hydrogel extract, and the toxicity of the hydrogel and the proliferation trend of the cells in the extract were evaluated by CCK-8 assays. In addition, cells were seeded onto the hydrogel, and the death and growth morphology of the cells on the gel was detected by Live/Dead staining and SEM, respectively. From the detections, the survival

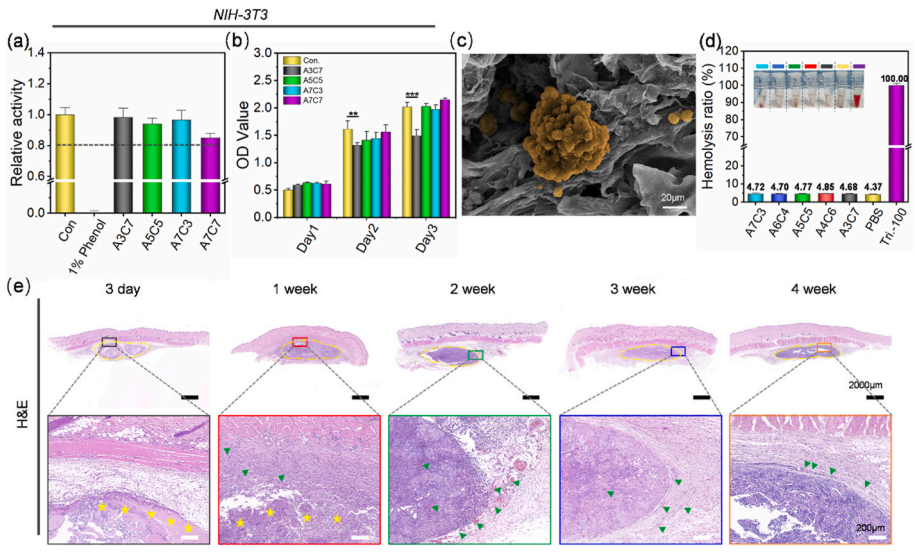

Fig. 4. Biocompatibility evaluation of the hydrogels. (a) Viability of the NIH-3T3 cells in hydrogel extracts. (b) Proliferation properties of the NIH-3T3 cells in hydrogel extract. (c) Morphology of the NIH-3T3 cells grown on A7C3 gel for 3 days by SEM (at 1000 ×). (d) The hemolysis rate of seven groups of hydrogels. The inset pictures showed the visualization of the hemolysis experiments after centrifugation, where the sediment at the bottom of the tubes is red blood cells. (e) H&E staining of the hydrogel and surrounding tissues after hydrogel injection into the subcutaneous of rats at 3,7, 14, 21 and 28 days. (The yellow dashed box indicates the hydrogel in the subcutaneous membrane capsule. The green "Δ" mark the blood vessels, and the yellow "☆ " indicates the hydrogel in the membrane capsule).

rate of cells in all groups in the extracts was greater than 80% after 24h of incubation in the extracts, i.e., the extracts were not significantly toxic (Fig. 4a). According to the absorbance from day 1 to day 3, the cells in the extracts showed an overall trend of proliferation over time. On day 1, the gel group showed a faster proliferation rate than the TCP group. On days 2 and 3, the proliferation trend of the hydrogel group was similar to that of the TCP group, with no significant difference, except for the A3C7 group (Fig. 4b). After the NIH-3T3 cells were inoculated onto the surface of the hydrogels with various mass percentages for 3 days, the Live/Dead staining confirmed that the cells did not undergo significant death (Fig. S5). The growth morphology of cells incubated on the hydrogels for 3 days was observed by SEM. The growth pattern of the cells on the hydrogel showed that the cells were round and grew in an aggregated manner. Cytocompatibility evaluation confirmed that the hydrogel had no significantly cytotoxic; the low affinity of the hydrogel predicts the adhesion prevention properties of the gel.

A prerequisite for materials used for hemostasis is good hemocompatibility. Thus, the hemocompatibility of the hydrogels was assessed by an *in vitro* hemolysis test using 5% rabbit blood dilution. The test results showed the macroscopic color of all five hydrogels was pale yellow, similar to the N.C. groups (PBS), while the P.C. groups (0.1% TrtonX-100) had a bright red color (inset in Fig. 5d). The hemolysis rate of each group of the hydrogels was less than 5%, closed to that of the N.C. groups and much lower than that of P.C. groups (Fig. 5d). The gel exhibited good hemocompatibility.

Good histocompatibility is a desirable property for implantable materials. The histocompatibility of the hydrogels was assessed by subcutaneous implantation experiments in rats. Specifically, 100uL A7C3 gel was implanted subcutaneously in rats (Figs. S6a and b), and the gel and tissues surrounded were harvested for pathological analysis on days 3, 7, 14, 21 and 28, respectively. After 7 days of injection, there was no obvious redness, swelling and suppuration in the tissues around the hydrogel from the macrographs (Fig. S6c). From the H&E staining of skin and subcutaneous hydrogel, on the 3rd day, only a small amount of mononuclear inflammatory cells was found to be present at the interface between hydrogel and tissue; However, a significant infiltration of inflammatory cells was observed around and inside the hydrogel 7 days after injection, which is the normal inflammatory response of the body to foreign implants. By day 14, the number of inflammatory cells had begun to decrease. No significant inflammatory cells were found in the hydrogel or surrounding tissues at days 21 and 28 (Fig. 5e). The number of blood vessels in the tissue around the hydrogel also showed a tendency of first increasing and then decreasing, consistent with the occurrence of inflammatory cells and with previous reports of the relationship between inflammation and angiogenesis [46,47].

Furthermore, to determine the maximum retention time of the hydrogels *in vivo*, we have detected their degradation *in vivo* dynamically by Magnetic Resonance Imaging (NMRI) technique *in situ* (Fig. S7a). As shown, the hydrogels had retained *in vivo* for as long as 20 weeks, with the residual volume being about 1/5 of the initial volume (Fig. S7b). This suggested that the biomacromolecule-based hydrogels may be degraded *in vivo* by endogenous enzymes such as hyaluronidase or chondroitinase, though the process is relatively long. On the other hand, it also suggested that the prepared hydrogels can persist *in vivo* for a long time without affecting the survival of the animals.

In conclusion, the biocompatibility test demonstrated that the hydrogel was not significantly cytotoxic, did not cause significant hemolysis, and exhibited a mild inflammatory response after implantation, indicating that the gel has good biocompatibility and is safe for use *in vivo*.

2.4. The uplifting and sealing effect of the multifunctional in-situ Hydrogel

2.4.1. Viscosity of a single component

The viscosity of the single component of the hydrogel was detected in

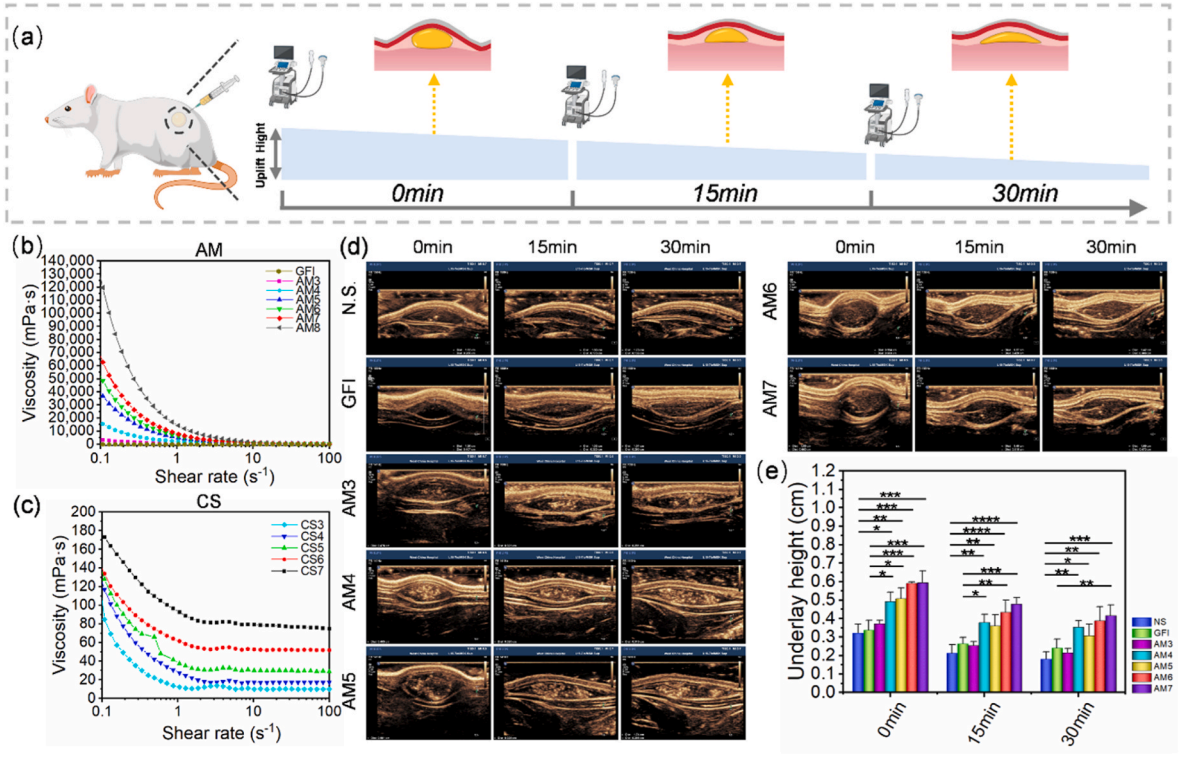

Fig. 5. Viscosity of a single hydrogel component and its effect on the subcutaneous uplift effect in rats. (a) Schematic diagram of the process of subcutaneous injection of SFC and ultrasonic detection in rats. (b) Viscosity curves of the GFI and AM*x* ($x = 3, 4, 5, 6, 7, 8$) solutions. (c) Viscosity curves of the CS*y* ($y = 3, 4, 5, 6, 7$) solutions. (d) Ultrasonic detection of the subcutaneous uplift effect of the NS, GFI and AM*x* ($x = 3, 4, 5, 6, 7, 8$) solutions in rats. (e) Statistics of the subcutaneous uplift height after submucosal injection in each group (n = 3) (*$P < 0.05$, **$P < 0.01$, ***$P < 0.001$, ****$P < 0.0001$, *ns*: no significant difference).

order to preferably select an appropriate component for submucosal injection. The viscosity curves are shown in Fig. 5b and c. From the viscosity curves, the viscosity of both solutions decreased with increasing shear rate, exhibiting typical shear thinning characteristics of non-Newtonian fluids. And the viscosity values of AM*x* (*x* = 3, 4, 5, 6, 7, 8) solutions were much larger than that of CS*x* (*x* = 3, 4, 5, 6, 7, 8) solution, as well as glycerol fructose injection (GFI) (Fig. 5b). However, when the mass fraction of AM reached 8 wt% (AM8), the viscosity of the solution increases sharply, which may be due to the increase of the viscosity of the solution with the increase of the content of AM, preventing the solvent molecules from entering the interior of the material, making the overall viscosity of the solution increase due to inadequate AM dissolution. Yet, viscous fluid is essential to reduce the spread of submucosal injection liquid. When performing endoscopic submucosal injection, the low-viscosity solution will spread rapidly in the submucosa after injection, which is not conducive to subsequent surgical operations, while the highly viscous solution may clog the needle. Therefore, according to the static viscosity values and viscosity curve trends of AM and CS solutions, the viscosity of AM solution is significantly larger than that of CS solution, which is more suitable for SFC.

2.4.2. Evaluation of uplift effect of AM solution

According to the 3R principle of experimental animal welfare, i.e., Replacement, Reduction and Refinement, the evaluation of the uplift effect of AM solution in the subcutaneous of rats was used to replace that of the effect in canine esophageal mucosa model to optimize the appropriate concentration of AM solution for subsequent canine esophageal ESD. And the process of subcutaneous i

njection of SFC materials and ultrasonic detection ain rats is shown as the schematic diagram in Fig. 5a. Specifically, 100 μL of each concentration of AM*x* (*x* = 3, 4, 5, 6, 7) solution was injected into the subcutaneous of the rats, and the uplift height was detected by ultrasonic at the initial (*T0* = 0 min) and 15min and 30min after injection, respectively, to evaluate the change of uplift height with time for different concentrations of AM solution (Fig. 5d). The saline (N.S.) and GFI were used as controls. It is evident from the figures that the initial (T_0 = 0 min) uplift height increased with the percentage of AM, where the uplift height is 0.48 ± 0.08 cm at concentrations of 4 wt%, higher than that of the N.S. and GFI groups (0.32 ± 0.05 cm and 0.34 ± 0.05 cm, respectively) (Fig. 4e). 30 min after injection, the AM7 group still maintained a significant uplift height of 0.42 ± 0.06 cm, much higher than the N.S. and GFI groups. Ultrasonic detection of the subcutaneous uplift height of AM solution showed that the 7 wt% AM (AM7) solution can maintain better uplift height and duration subcutaneously in rats compared to clinically used N.S. and GFI injections. Combined with the component viscosity detection and ultrasonic detection of the uplift height in rat subcutaneous, the AM component has a higher viscosity than the CS solution, and the 7 wt% of the AM component (AM7) has the optimal viscosity and is suitable for use as SFC material. In contrast, the CS3 component with lower viscosity is suitable for spraying on the post-ESD wound and gelled with residue and/or backfill AM7 solution in wound. In this section, the combination of AM7 and CS3 optimized according to the actual demands of ESD is consistent with the A7C3 gel combination optimized by physicochemical properties in the previous section.

2.4.3. Hemostatic ability of hydrogels in vivo/in vitro

In trauma and emergencies, hemostasis is the first step in the repair of injured tissue, and hemostatic materials are necessary to the prevention of uncontrolled bleeding during surgery [12]. As a wound sealant, the hydrogel achieved a good balance between adhesion strength and biocompatibility, which was verified from the results of adhesion tests (Fig. 3) and biocompatibility (Fig. 4). Therefore, we further investigated the *in vivo/in vitro* hemostatic properties of the *in-situ* hydrogel and subsequently explored the potential application of hydrogels in canine esophageal closure/wound healing. The hemostatic behavior of the *in-situ* hydrogel was detected by employing the rabbit liver trauma model (*in vitro*) (Fig. 6a) and an endoscopy-assisted minimally invasive rabbit liver hemostasis model (*in vivo*) (Fig. 6e). The untreated group and commercially available fibrin glue were served as controls. The amount of blood loss and bleeding time were recorded. In the rabbit liver trauma model 1 (Fig. 6a), the untreated group showed a larger blood stain on the filter paper, with the liver blood loss being 0.945 ± 0.161 g (Fig. 6b). The fibrin glue group had a smaller blood stain area on the filter paper than both the untreated group and the A7C3 gel group, with a blood loss of 0.603 ± 0.040 g. The blood-stained area in the A7C3 gel group was smaller than that of untreated group but slightly larger than that of the fibrin glue group, with the blood loss of 0.658 ± 0.075 g (Fig. 6c). The untreated group had the longest hemostasis time of 152.7 ± 17.5s, much longer than the fibrin glue and A7C3 gel groups, while the hemostasis time between these two groups was 78.00 ± 29.21s and 91.33 ± 16.65s, respectively, with no significant difference (Fig. 6d).

In clinical practice, laparoscopic surgery is increasingly being used as an alternative to open laparotomy. Here, we performed minimally invasive surgery on both sides of the midline of the rabbit's abdomen, and established liver-injury model under portable endoscope guidance, along with endoscopically assisted targeted delivery of hydrogel, to explore the hemostatic ability of the *in-situ* hydrogel for *in vivo* injury (Fig. 6e, f and g). Commercially available fibrin glue was used as control. The liver was harvested one week after the surgery to observe the wound healing. As shown in the results, no blood exudation from the wound was observed after sealing with the *in-situ* gel and fibrin glue, respectively, and both the A7C3 gel and fibrin glue showed a good sealing effect (Fig. 6h and i). One week after the surgery, it can be seen that the wounds in both groups have healed, and the scar at the healing site is of the same degree.

The hemostasis test of the rabbit liver *in vitro/in vivo* showed that the A7C3 gel achieved excellent closure and hemostatic effect on the bleeding wounds, and the hemostatic effect was consistent with that of fibrin glue. We inferred that this rapid hemostatic ability of *in-situ* hydrogels may be attributed to the rapid click-crosslinked gel-forming ability of the hydrogels as well as its tissue adhesion properties. Furthermore, no tissue adhesion was occurred in the rabbit liver *in vivo* hemostasis model due to the low cell affinity property of the hydrogel (Fig. 4c). Hemostatic tests demonstrated that A7C3 *in-situ* hydrogel can be used as a sealant and hemostatic agent in wounds after injury has occurred.

2.5. Evaluation of the Tow-component in-situ Hydrogel on canine esophageal ESD

2.5.1. Mucosal uplift effect of the AM7 solution

The AM7 solution was used as SFC for ESD in the canine esophagus and its uplift effect in the esophageal submucosa was evaluated. The canine esophageal ESD surgery was performed with the assistance of a portable endoscopic system (Fig. 7a). Briefly, a sterile rubber band (1.5 cm in diameter) was placed in the esophagus with a biopsy forceps to simulate the localization of the lesion, and marked around the "lesion" with an electric knife, then 50 μL of AM solution was injected into the submucosa of the marked area using a disposable endoscopic injection needle. The change of the mucosa uplift height was observed by the implanted ruler (Fig. 7b). Clinical mucosal injection GFI was used as a control. As seen in Fig. 7c, the mucosa showed a broad-based peak elevation after GFI injection. Whereas after injection of AM7 solution, the mucosa showed a convex peak elevation. After 15min, the mucosal bulge peak in the GFI group tended to be flattened due to the diffusion of GFI submucosal, accompanied by the appearance of mucosal folds, while the bulge height in the AM7 group did not change significantly. After 30 min, the mucosal bulge peak of the GFI group disappeared with mucosal folds evident, while the AM7 solution group still maintained a good mucosal uplift effect after injection, with no significant difference

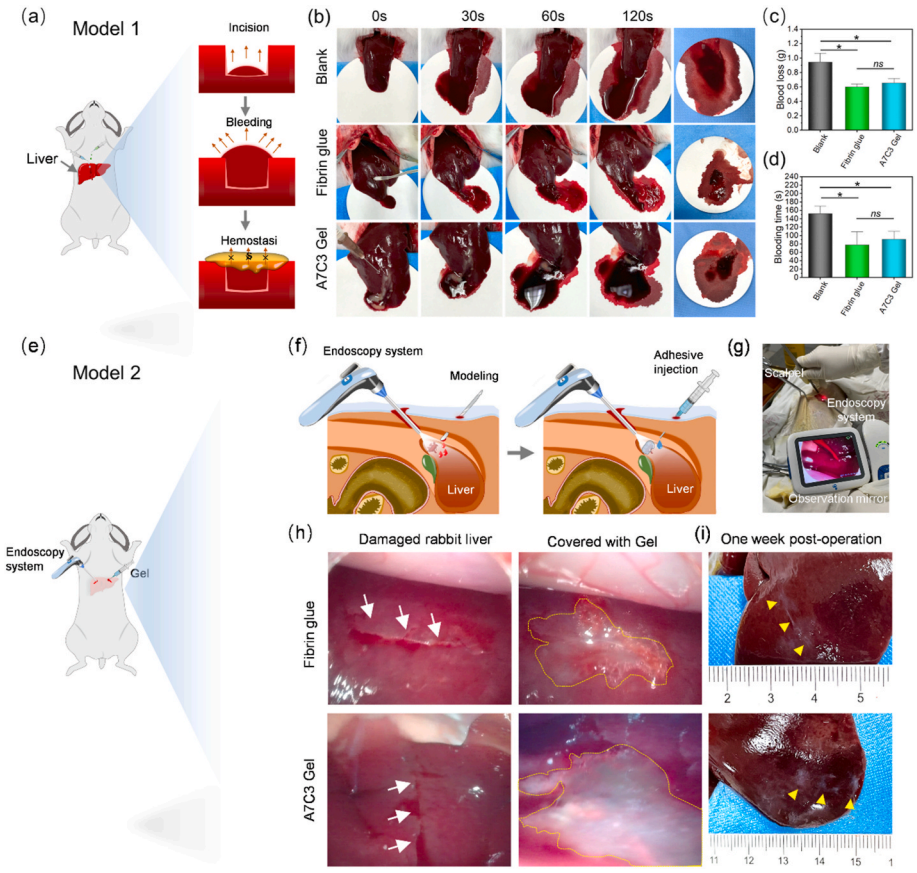

Fig. 6. (a) Schematic diagram of the surgical procedure for hemostasis of the rabbit liver (*in vitro*). (b) Diagram of hemostatic effect of untreated group and after hemostasis with fibrin glue and hydrogel respectively. (c) Statistics of blood loss after hemostasis in control and gel groups. (d) Statistics of hemostasis time in control and gel groups (n = 5). (e, f) Schematic diagram of endoscopically assisted hemostasis in rabbit liver model (*in vivo*). (g) Operation diagram of endoscopy-assisted rabbit liver hemostasis experiment. (h) Endoscopic modeling of rabbit liver hemorrhage and morphology after wound closure with fibrin glue and A7C3 gel (White arrows indicate postoperative wounds; Yellow dashed boxes indicate the wound after hydrogel closure). (i) Liver healing one week after surgery (The yellow "△" in the figure indicate the healed wound) (*$P < 0.05$, *ns*: no significant difference).

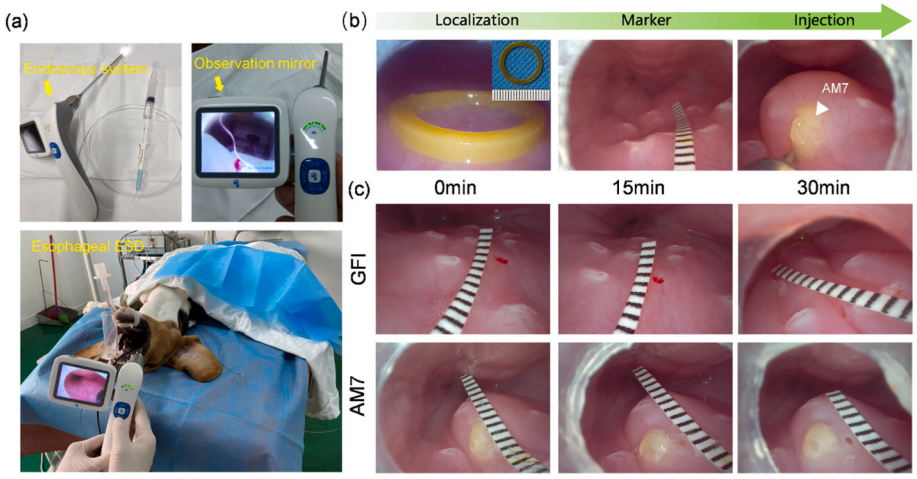

Fig. 7. Procedure of ESD in canine esophagus and the evaluation of the effect of AM solution on submucosal uplift of canine esophagus. (a) Portable endoscopy pictures and surgical procedure picture of canine esophageal ESD. (b) ESD submucosal injection procedure, including lesion localization, electrotome marking, and submucosal injection of AM7 solution. (c) Morphological diagram of the effect of GFI and AM7 solutions as SFC in the submucosa and photographs of the uplift height of the mucosal layer by GFI and AM7 solutions at 0, 15, and 30 min.

compared with the initial height.

In the experiment on the effect of submucosal injection in canine, it can be seen that GFI dissipates rapidly when injected into the submucosa due to the low viscosity, which is consistent with its clinical use effect, while the AM7 solution developed in this study maintains a long-lasting mucosal uplift height (>30 min) after injection due to its high viscosity. Therefore, AM7 solution has a great prospect as a potential alternative to submucosal injection in ESD.

2.5.2. *Application of in-situ gel in canine esophageal ESD*

In the application of A7C3 gel in canine esophageal ESD, AM7 solution is used as SFC material, followed by CS3 solution sprayed on the wound after ESD, which gelatinized *in situ* with AM7 solution to seal the wound. The surgical schematic and procedure are shown in Fig. 8a and Video 2. Specifically, AM7 solution was firstly injected into the submucosa marked "lesion" area through a disposable endoscopic injection needle (Fig. 8b), and then the mucosal layer of the lesion area was dissected with an electrocoagulation knife, at which point the exposed AM7 solution in the submucosa was visible (Fig. 8c). Subsequently, the CS3 solution was sprayed on the wound, which can be immediately gelatinized *in situ* when in contact with the AM7 solution, separating the wound from the GI environment. In contrast, for lesions occurring in the submucosa, such as early submucosal tumors, blood stains and residual SFC material (AM7 solution) should be removed from the wound to

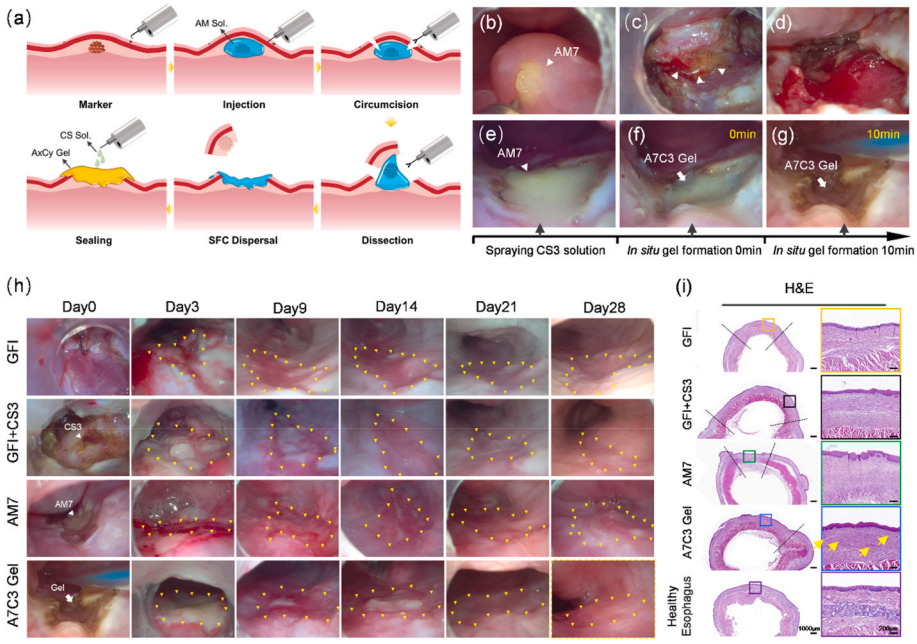

Fig. 8. Evaluation of the multifunctional *in-situ* hydrogel in canine esophageal ESD. (a) Schematic diagram of the canine esophageal ESD procedure. (b) Injection of AM7 solution into the submucosa of the canine esophagus (The white "△" indicates the AM7 solution returned after needle withdrawn).(c) Mucosal dissection (The white "△" indicates the exposure of AM7 solution after mucosal dissection). (d) Removal of blood stains and SFC materials from the wound. (e) Fulfilled the wound with AM7 solution, and then spray with CS3 solution. (f) Gel morphology after CS3 solution in contact with AM7 solution at the wound (0 min) (White arrows indicate the A7C3 gel). (g) Morphology of the hydrogel after gelling and stabilizing in the wound (10 min). (h) Observation of wound healing on days 0, 3, 9, 14, 21 and 28 after ESD (Yellow "△" indicates the border of the wound). (i) H&E staining of esophageal tissues harvested on day 28 after ESD (Yellow arrows indicate the glands in the mucosa).

provide a clear surgical view (Fig. 8d and e), followed by filling the wound with fresh AM7 solution to facilitate gel formation (Fig. 8f and g). The postoperative wound closure ability of the *in-situ* gel may result from the rapid click-crosslinked ability between the AM solution and the CS solution, and tissue adhesion properties as previously described.

Supplementary video related to this article can be found at https://doi.org/10.1016/j.bioactmat.2023.04.015

The experimental grouping of canine esophageal ESD is shown in Fig. S8a, and all esophageal ESD surgeries were performed according to the procedure described above. The wound healing was observed with a portable endoscope on the 3rd, 9th, 14th, and 28th days after ESD (Fig. 8h). From the observations, the wounds of GFI, GFI + CS3 and AM7 groups showed obvious redness and inflammation on the 3rd day post operation due to wound exposure, and inadequate granulation tissue growth in the wound and did not fully fill the wounds. On day 9, wounds in the GFI, GFI + CS3, and AM7 groups showed varying degrees of scar tissue formation, which persisted until day 28. In contrast, the wounds in the A7C3 gel group did not exhibit significant redness and swelling, and were adequately filled with granulation tissue by day 3 post-operatively. Similarly, in group A7C3, the wound was well filled with granulation tissue on postoperative day 9. On day 14, the granulation matured and the wound looked flat. On day 21, the wound was completely healed without obvious scar formation. On day 28, the wound was flat and the morphology did not differ significantly from normal esophageal tissue. The esophageal tissues of the five groups were harvested on the 28th day after the ESD (Figs. S8b–S8g). Morphologically, it can be seen that compared with normal esophageal tissue (Fig. S8g), the A7C3 gel group (Fig. S8b-①, e−②, f-①) showed a flat wound surface without obvious scars, while the other three groups all had scars of different degrees, indicating that wound closure after ESD in canine esophagus facilitates healing.

The better healing and weaker scar formation exhibited by the gel-sealed wounds after ESD may be attributed to the fact that the gel isolates the wounds from direct contact with the environmental noxious factors in GI tract, reducing the impact of environmental noxious factors on wound repair.

2.5.3. *Healing promoting effects of the hydrogels in canine esophageal ESD model*

The wound healing process after esophageal ESD also includes re-epithelialization and ECM remodeling. Therefore, we evaluated the effect of *in-situ* hydrogel A7C3 on these processes after ESD surgery. The esophageal tissues were collected on day 28 after ESD, and stained for H&E. According to the staining results, the wounds in all groups were completely healed and re-epithelialization on the 28th day (Fig. 8i). However, there were significant differences in the structure of mucosal lamina propria in the healed area between groups. Compared with normal esophageal tissue, the lamina propria of the esophageal mucosa in GFI and GFI + CS3 groups was thinner, and the collagen fibers were loosely arranged and wavy, indicating severe fibrosis in the ECM reconstruction during the wound healing process. Whereas, the mucosal lamina propria of the AM7 group was dense, with obvious stromal deposition. By contrast, the mucosal lamina propria of the A7C3 gel group was moderately thick, with blood vessels and small glandular structures contained in it (yellow arrows in Fig. 8i), which was close to the structure of mucosal lamina propria of healthy esophageal tissue.

The ratio of type I/III collagen and its arrangement during wound healing has an important effect on the scar-free healing of the tissue [48]. Sirius red staining was performed on esophageal tissues of each group on the 28th day after surgery. As shown in Fig. 9a, Sirius red staining of the damaged area in the GFI, AM7 and GFI + CS3 groups showed a predominance of type I collagen, and the arrangement and morphology of collagen fibril were consistent with that observed in H&E staining. In contrast, in the A7C3 gel group, type III collagen was increased (green staining), and type I and III collagen were arranged interchangeably in an irregular manner, which was similar to that of normal esophageal tissues. The collagen architecture of the wounds in each group was further assessed using CT-FIRE and CurveAlign software algorithms, which were developed to analyze collagen fiber properties in histological images [49,50]. From the fiber structure analysis, collagen fiber in the GFI, AM7 and GFI + CS3 groups exhibited significant elongation and increased unidirectional alignment, whereas collagen fiber in A7C3 gel groups, in contrast, presented a basket weave-like collagen fiber network similar to that of health esophagus with a wide range of metrics. Specifically, both A7C3 gel-treated esophagus and the normal esophagus exhibited misalignment, and a reduction in fiber length, along with an increased in the number of shorter collagen fibers (Fig. 9b). Although there are many factors that affect the process of re-epithelialization and scar formation after injury, but in our study, the postoperative wound closure with hydrogel

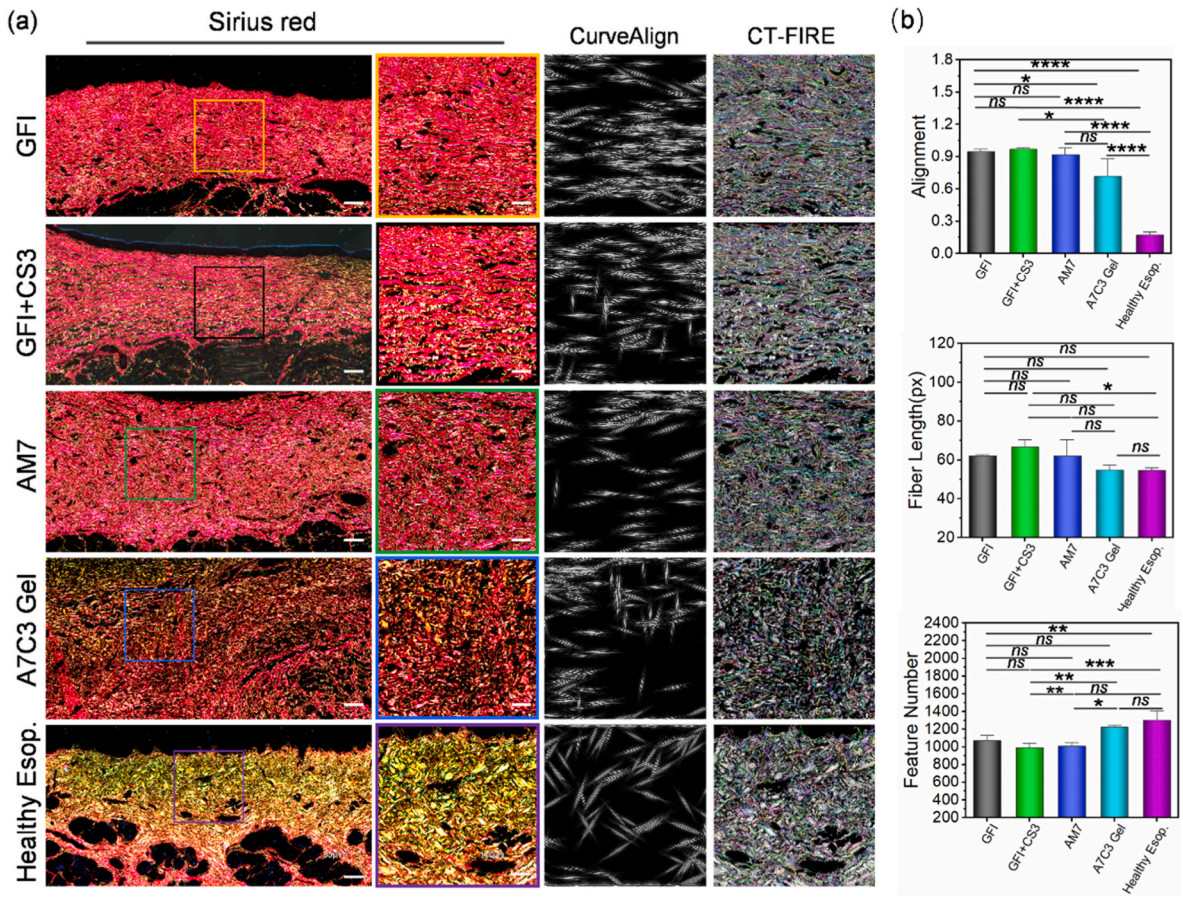

Fig. 9. Type of collagen formation after wound healing. (a) Sirius red staining of the esophageal tissue on day 28 after ESD (red for type I collagen, green for type III collagen), and quantification of five groups of wounds by alignment (CurveAlign, 3rd column) and CT-FIRE (4th column). (b) Quantification of the different collagen fiber network characteristics, alignment, fiber length and number among the five groups. (*$P < 0.05$, **$P < 0.01$, ***$P < 0.001$, *ns*: no significant difference).

accelerated the healing process and reduced the occurrence of fibrosis in ECM formation. A possible reason for the better repair effect exhibited after closure of post-ESD wounds in the canine esophagus with A7C3 gel is that the gel reduces the exposure of the wounds to digestive juices and food, thus preventing bacterial infection and inflammation of the wounds, and ultimately reducing the fibrosis and scar formation during the healing process.

In summary, the two-component *in-situ* hydrogel we prepared fulfilled the initial expectations for use as mucosa uplift, wound closure and accelerated healing in ESD, but there are still some shortcomings in the study. Limited by the acquisition of experimental dogs and specific antibodies for relevant pathological indexes, we have not been able to conduct more exploration on the mechanism of hydrogel promoting wound repair after ESD. In the follow-up study, we will further explore the principle of the promoting repair effect of the hydrogel and further validate the application effect of this multifunctional *in-situ* hydrogel in GI tract ESD in larger experimental animal.

3. Conclusion

In this study, a series of rapid-gelling A*x*C*y* (*x, y* = 3, 4, 5, 6, 7) hydrogels were prepared by mixing two derivatives, ADA-Mal (AM) and CMCS-SH (CS), based on the Michael addition reaction in "click" chemistry and Schiff base reaction, etc. The developed *in-situ* gel simultaneously solves the problems of easy diffusion of submucosal injection materials and postoperative wound closure in clinical ESD. The A7C3 gel has the characteristics of short gel-forming time, good tissue adhesion, better physicochemical performance and biological properties (cytocompatibility, hemocompatibility and histocompatibility), which can be used as a rapid wound sealant. The single component of the A7C3 gel, AM7 (7 wt%) solution, is used as a submucosal injection solution due to its suitable viscosity, while the lower viscosity CS3 (3 wt%) solution is used for postoperative spraying on the wound surface and cross-linking with AM7 solution to form a gel and seal the wound. Studies have confirmed that AM7 solution can maintain sufficient uplift height and duration without dissipation in the rat subcutis as well as in the canine esophageal submucosa, and therefore can be used as an alternative option to clinical use SFC for ESD. When the sprayed CS3 solution comes in contact with the exposed or backfilled AM7 solution, the A7C3 gel is formed immediately based on click-crosslinked, which acts to seal the wound and stop bleeding. *In vivo* and *in vitro* rabbit liver hemostatic experiments confirmed that A7C3 *in-situ* hydrogel has good wound sealing ability and hemostatic effect, which is close to that of commercial fibrin glue. In addition, the results of H&E staining and Sirius red staining of healed esophageal tissues revealed that postoperative wounds sealed by hydrogels exhibited better healing effect, as well as lower fibrosis and scar formation, and the recovered esophageal tissue was closer to the natural tissue structure. In conclusion, the multifunctional *in-situ* hydrogel prepared in this study provides a promising candidate for the clinical treatment of ESD.

4. Experimental section

***Preparation of the Hydrogels*:** ADA-Mal (abbr. to AM) and CMCS-SH (abbr. to CS), of which the preparation methods are described in detail in the supplementary materials, were respectively dissolved in phosphate buffer solution (PBS) and $Na_2B_4O_7$ solution (0.01 M) to obtain the AM*x* and CS*y* (*x, y* = 3, 4, 5, 6, 7) solution, where *x* and *y* are the mass

percentage of the solute. The gel is formed once the two solutions are mixed in a certain proportion. Thereinto, a series of hydrogels, namely A*x*C*y* (*x, y* = 3, 4, 5, 6, 7), can be formed with the mixing of AM*x* and CS*y*.

***Gelation Time*:** The gelation time of A*x*C*y* (*x, y* = 3, 4, 5, 6, 7) was measured by a tube inversion method. Briefly, 500 μL of AM*x* and CS*y* (*x, y* = 3, 4, 5, 6, 7) solution was added into a ep tube (5 mL) in order followed by adding a rotor (type-C, 0.5 cm), then placed on a magnetic agitator (Sile Instruments Co., Ltd. Shanghai, China), stirred at 120 rpm. The tube was inverted every 3 s until the hydrogel was formed at the bottom of ep tube and did not fall during inversion, when the time is defined as the time of hydrogel formation, and the final gelation time was recorded (n = 5).

***Microstructure Observation*:** The morphology of the hydrogels was characterized with a scanning electron microscope (SEM, EVO MA10, ZEISS, Germany). Prior to the test, the gel was lyophilized and quenched with liquid nitrogen to exposed the inner structure. The cross-section of the lyophilized gel was observed by SEM after gold sputtering treatment. The pore diameters were measured with Image J software (n = 20 visual fields).

***Swelling Property Study*:** Swelling property of the A*x*C*y* (*x, y* = 3, 4, 5, 6, 7) is defined with the swelling ratio. For swelling test, cylindric hydrogels was weighed and immersed in PBS (10 mL) at 37 °C with shaking at 60 rpm in a shaker. At the predetermined time, the hydrogel was taken out and weighed after blotting the extra water. The process was repeated until the hydrogels reached equilibrium (n = 3). The swelling ratio (%) is calculated with the following formula: $Swelling\ Ratio\ (\%) = (W_t - W_0)/W_0 \times 100\%$, where W_0 and W_t represent the weight of the hydrogel at the initial and pre-set time, respectively.

***Rheological Properties Study*:** The rheological properties of the A*x*C*y* (*x, y* = 3, 4, 5, 6, 7) were measured using a rotational rheometer (Physica MCR302, Anton Paar, Austria). All tests were carried out with a cone plate rotor (CP25-3, diameter = 25 mm, angle = 3°) and a 500 μm gap size at 37 °C. The amplitude sweep mode (0.1–500%, 1 Hz) and frequency sweep mode (1%, 0.1–10 Hz) were conducted to assess the rheological property of the hydrogels, and the rheological curve was recorded. Self-healing was assessed by alternating the step-strain sweep mode at a fixed frequency of 1 Hz and temperature of 37 °C, with oscillatory strains switching back and forth between 1% and 300% at an interval of 50 s.

***Adhesive Behavior Study*:** The adhesive behavior of the hydrogels was evaluated by *in vitro* adhesion test and bursting test. Fresh porcine skin stripped of excessive fat was cut into long strips (5 cm × 3 cm) and incubated in PBS (37 °C) for 30 min before the test. 200 μL of hydrogel was gelled *in situ* on the surface of porcine skin. After hydrogel stabilization, repeatedly stretched, bent and twisted the skin to observe the adhesion of the hydrogel to the porcine skin. Subsequently, the strips were separately soaked in PBS (pH = 7.4) and 1 M HCl solution (pH = 1.2) at 37 °C and shook at 60 rpm for 24, 48 and 72 h, and subjected to twisting, bending and stretching similarly as before to observe the adhesion of the hydrogels. Adhesion of the hydrogel to the irregular wounds by gelling the *in-situ* gel on the surface of the star-shaped wound, then the boundary of the hydrogel in contact with the wound was rinsed with running water to observe the gel shedding. The burst pressure was performed on a porcine skin with a hole in the center. Briefly, a defect (2 mm × 1 mm) was made on the fixed porcine skin. 100 μL of A7C3 hydrogel was gelled *in situ* onto on a defect (2 mm × 1 mm) previously made on the surface of the pigskin fixed on the detection device, then the water in the syringe was slowly pushed into the chamber of the experimental device until the hydrogel adhering to the pigskin groove surface is broken. The maximum pressure (kPa) was recorded as the burst pressure. Fibrin glue was used as the control. All tests were repeated for 3 times (n = 3). Lap-shear test was performed to evaluate the tissue adhesion forces of the hydrogels. Briefly, tissues were coated on PMMA plates with α-cyanoacrylate ethyl ester-based glue before the testing, and the A7C3 hydrogel was placed between two PMMA plates coated with the tissues and fixed for 10 min. The two PMMA plates were then placed into an universal testing machine (Instron 5967, USA) for tensile loading at a strain rate of 1 mm/s. The hydrogel adhesion strength was determined at the point of detachment.

***Biocompatibility Study*:** The cytocompatibility, hemocompatibility and histocompatibility of the hydrogels were evaluated respectively. Detailed methods are described in the Supporting Information.

Viscosity Study: The viscosities of the AM and CS solutions were tested as follows: AM and CS solutions of different mass percentages (wt %) were prepared. A rotational rheometer (MCR302, Anton Paar, Austria) with a 50 mm plate rotor (PP50) was used as the test component. The test parameters were set as follows: the gap between the upper and lower plates was set as 0.25 mm, and the platform temperature was set as 37 °C. The shear rate was set as 0.1–100 rad/s. The viscosity curves of AM*x* and CS*y* (*x, y* = 3, 4, 5, 6, 7) were tested in the rotating mode. The glycerol fructose injection (GFI) was used as the control.

***Subcutaneous Uplift Effect Study*:** AM*x* (*x* = 3, 4, 5, 6, 7) solutions were used as submucosal fluid cushion (SFC) materials, and the change of the subcutaneous uplift height over time in rats was detected by ultrasound detector (PHILIPS IU22, Philips Electronics Group, The Netherlands). Specifically, SD rats weighing 300–350 g were anesthetized with 1.5 wt% pentobarbital sodium solution (200 mg mL^{-1}). The back area was depilated to expose both sides of the skin, and the injection sites were marked. 100 μL of AM*x* (*x* = 3, 4, 5, 6, 7) solution was injected subcutaneously into the rat and the height of skin uplifting was measured with an ultrasonic detector, recorded and marked as $t = 0$ min. Three parallel injection points were set up in each group (n = 3), with saline and GFI as controls. The skin uplift height was recorded at 15 min and 30 min, respectively.

***Hemostasis Ability Study*:** The hemostatic properties of the hydrogel were assessed by rabbit liver hemostasis assay (*in vitro*), and endoscopy-assisted minimally invasive hemostasis assay (*in vivo*) [51]. Detailed procedures are described in the Supporting Information.

***Canine Esophageal ESD*:** Healthy adult Beagle (weighing 10–15 kg each, n = 5) were selected and fasted for food and water for 6 h prior the surgery. All canine procedures were approved by the Experimental Animal Ethics Committee of the West China Hospital, Sichuan University (Approval No. 20220225127). Detailed experimental groupings and surgical procedures are described in the Supplementary material. These experimental dogs were fed through a nasal cannula for the first three days after surgery and then fed a normal diet until euthanasia. The canine esophagus was examined with a portable endoscope on postoperative days 3, 9, 14, 21, and 28 to observe inflammation, granulation, and wound closure in the trabecular area. Euthanasia was carried out on day 28, and esophageal tissues were harvested for follow-up examination.

***Histological Test*:** The wound tissues harvested were fixed and embedded in paraffin, sectioned into slices, and subjected to H&E staining to evaluate the pathological status and healing process. Sirius red staining was used to evaluate the expression levels of COL I and COL III. The detailed procedures are described in the Supporting Information.

***Statistical analyses*:** Statistical analyses were carried out in Prism8 (GraphPad) using paired or unpaired Student's *t* tests, and one-way or two-way analysis of variance (ANOVA) with Tukey's multiple comparisons test. All data are presented as means ± SD. $P < 0.05$ was considered statistically significant.

CRediT authorship contribution statement

Xiong-Xin Lei: Conceptualization, Data curation, Formal analysis, Investigation, Methodology, Resources, Software, Writing – original draft. **Juan-Juan Hu:** Data curation, Formal analysis, Investigation, Resources, Project administration, Writing – review & editing. **Chen-Yu Zou:** Data curation, Formal analysis, Investigation. **Yan-Lin Jiang:** Data curation, Resources, Investigation. **Long-Mei Zhao:** Data curation,

Formal analysis, Investigation. **Xiu-Zhen Zhang:** Data curation, Investigation. **Ya-Xing Li:** Data curation, Investigation. **An-Ni Peng:** Data curation. **Yu-Ting Song:** Data curation, Methodology. **Li-Ping Huang:** Data curation, Formal analysis, Methodology, Resources, Software, Supervision, Validation. **Jesse Li-Ling:** Data curation, Formal analysis, Writing – review & editing. **Hui-Qi Xie:** Conceptualization, Data curation, Formal analysis, Funding acquisition, Project administration, Resources, Supervision, Validation, Visualization, Writing – review & editing.

Declaration of competing interest

This manuscript has been approved by all coauthors. It has not been published or presented elsewhere in part or in entirety and is not under consideration by another journal. We have read and understood your journal's policies, and we believe that neither the manuscript nor the study violates any of these. There are no conflicts of interest to declare.

Acknowledgements

This work was supported by the National Natural Science Foundation of China (Grant No. 32171351), the "1.3.5" Project for Disciplines of Excellence, West China Hospital, Sichuan University (Grant No. ZYJC18002), and China Postdoctoral Science Foundation (2022M722277).

Appendix A. Supplementary data

Supplementary data to this article can be found online at https://doi.org/10.1016/j.bioactmat.2023.04.015.

References

[1] H. Sung, J. Ferlay, R.L. Siegel, M. Laversanne, I. Soerjomataram, A. Jemal, F. Bray, Global cancer statistics 2020: globocan estimates of incidence and mortality worldwide for 36 cancers in 185 countries, Ca - Cancer J. Clin. 71 (3) (2021) 209–249, https://doi.org/10.3322/caac.21660.

[2] T. Lambin, J. Rivory, T. Wallenhorst, R. Legros, F. Monzy, J. Jacques, M. Pioche, Endoscopic submucosal dissection: how to be more efficient? Endosc. Int. Open 9 (11) (2021) E1720–E1730, https://doi.org/10.1055/a-1554-3884.

[3] I. Saito, Y. Tsuji, Y. Sakaguchi, K. Niimi, S. Ono, S. Kodashima, N. Yamamichi, M. Fujishiro, K. Koike, Complications related to gastric endoscopic submucosal dissection and their managements, Clin. Endosc. 47 (5) (2014) 398–403, https://doi.org/10.5946/ce.2014.47.5.398.

[4] D. Jung, Y.H. Youn, J. Jahng, J.H. Kim, H. Park, Risk of electrocoagulation syndrome after endoscopic submucosal dissection in the colon and rectum, Endoscopy 45 (9) (2013) 714–717, https://doi.org/10.1055/s-0033-1344555.

[5] C.H. Yang, Y. Qiu, X. Li, R.H. Shi, Bleeding after endoscopic submucosal dissection of gastric lesions, J. Dig. Dis. 21 (3) (2020) 139–146, https://doi.org/10.1111/1751-2980.12850.

[6] T.R. Soong, J. Nayor, M.D. Stachler, M. Perencevich, K. Jajoo, J.R. Saltzman, N. I. Lindeman, A. Srivastava, Clinicopathologic and genetic characteristics of interval colorectal carcinomas favor origin from missed or incompletely excised precursors, Mod. Pathol. 32 (5) (2019) 666–674, https://doi.org/10.1038/s41379-018-0176-6.

[7] Y. Pang, J. Liu, Z.L. Moussa, J.E. Collins, S. McDonnell, A.M. Hayward, K. Jajoo, R. Langer, G. Traverso, Endoscopically injectable shear-thinning hydrogels facilitating polyp removal, Adv. Sci. 6 (19) (2019), 1901041, https://doi.org/10.1002/advs.201901041.

[8] S. Hirasaki, T. Kozu, H. Yamamoto, Y. Sano, N. Yahagi, T. Oyama, T. Shimoda, K. Sugano, H. Tajiri, T. Takekoshi, D. Saito, Usefulness and safety of 0.4% sodium hyaluronate solution as a submucosal fluid "cushion" for endoscopic resection of colorectal mucosal neoplasms: a prospective multi-center open-label trial, BMC Gastroenterol. 9 (1) (2009), https://doi.org/10.1186/1471-230x-9-1.

[9] J.J. Hyun, H.R. Chun, H.J. Chun, Y.T. Jeen, C.W. Baeck, S.K. Yu, Y.S. Kim, H.S. Lee, S.H. Um, S.W. Lee, J.H. Choi, C.D. Kim, H.S. Ryu, J.H. Hyun, Comparison of the characteristics of submucosal injection solutions used in endoscopic mucosal resection, Scand. J. Gastroenterol. 41 (4) (2006) 488–492, https://doi.org/10.1080/00365520500325994.

[10] T. Ishizuka, T. Hayashi, M. Ishihara, Y. Yoshizumi, S. Aiko, S. Nakamura, H. Yura, Y. Kanatani, Y. Nogami, T. Maehara, Submucosal injection for endoscopic mucosal resection, of photocrosslinkable chitosan hydrogel in dmem/f12 medium, Endoscopy 39 (5) (2007) 428–433, https://doi.org/10.1055/s-2007-966393.

[11] S. Speca, I. Giusti, F. Rieder, G. Latella, Cellular and molecular mechanisms of intestinal fibrosis, World J. Gastroenterol. 18 (28) (2012) 3635–3661, https://doi.org/10.3748/wjg.v18.i28.3635.

[12] I.O. Gordon, N. Agrawal, E. Willis, J.R. Goldblum, R. Lopez, D. Allende, X. Liu, D. Y. Patil, L. Yerian, F. El-Khider, C. Fiocchi, F. Rieder, Fibrosis in ulcerative colitis is directly linked to severity and chronicity of mucosal inflammation, Aliment. Pharmacol. Ther. 47 (7) (2018) 922–939, https://doi.org/10.1111/apt.14526.

[13] H. Maeda, F. Sasaki, Y. Morinaga, M. Kabayama, H. Iwaya, Y. Komaki, S. Arima, Y. Nasu, S. Tanoue, S. Hashimoto, S. Kanmura, A. Nishiguchi, T. Taguchi, A. Ido, Covering post-endoscopic submucosal dissection ulcers in miniature swine with hexanoyl (hx:C6) group-modified alkaline-treated gelatin porous film (hag) induces proper healing by decreasing inflammation and fibrosis, Digestion 102 (3) (2021) 415–427, https://doi.org/10.1159/000509056.

[14] T. Ohki, M. Yamato, M. Ota, R. Takagi, D. Murakami, M. Kondo, R. Sasaki, H. Namiki, T. Okano, M. Yamamoto, Prevention of esophageal stricture after endoscopic submucosal dissection using tissue-engineered cell sheets, Gastroenterol. 143 (3) (2012) 582–588 e582, https://doi.org/10.1053/j.gastro.2012.04.050.

[15] S. Aoki, Y. Sakata, R. Shimoda, T. Takezawa, A.O. Miyazaki, H. Kimura, M. Yamamoto, R. Iwakiri, K. Fujimoto, S. Toda, High-density collagen patch prevents stricture after endoscopic circumferential submucosal dissection of the esophagus: a porcine model, Gastrointest. Endosc. 85 (5) (2017) 1076–1085, https://doi.org/10.1016/j.gie.2016.10.012.

[16] G. Heidari, M. Hassanpour, F. Nejaddehbashi, M.R. Sarfjoo, S. Yousefiasl, E. Sharifi, A.B.T. Agarwal, A. Borzacchiello, E. Lagreca, C.D. Natale, N. Nikfarjam, Y. Vasseghian, Biosynthesized nanomaterials with antioxidant and antimicrobial properties, Mater. Chem. Horizons 1 (1) (2022) 35–48, https://doi.org/10.22128/mch.2022.553.1005.

[17] R. Kushwaha, S. Sharma, S. Kumar, A. Kumar, Biopolymers as topical haemostatic agents: current trends and technologies, Mater. Chem. Horizons 2 (1) (2023) 11–39, https://doi.org/10.22128/MCH.2022.612.1029.

[18] T. Yamashina, N. Uedo, M. Fujii, R. Ishihara, M. Mikamori, M. Motoori, M. Yano, H. Iishi, Delayed perforation after intralesional triamcinolone injection for esophageal stricture following endoscopic submucosal dissection, Endoscopy 45 (Suppl 2) (2013), https://doi.org/10.1055/s-0032-1326253. UCTN: E92.

[19] K. Takimoto, T. Toyonaga, K. Matsuyama, Endoscopic tissue shielding to prevent delayed perforation associated with endoscopic submucosal dissection for duodenal neoplasms, Endoscopy 44 (Suppl 2) (2012), https://doi.org/10.1055/s-0032-1325739. UCTN: E414-415.

[20] D. Kikuchi, T. Iizuka, K. Nomura, Y. Kuribayashi, M. Tanaka, S. Yamashita, T. Furuhata, A. Matsui, T. Mitani, S. Makino, S. Hoteya, Feasibility of autologous fibrin glue and polyglycolic acid sheets to prevent delayed bleeding after endoscopic submucosal dissection of gastric neoplasms in patients receiving antithrombotic therapy, Gastroenterol. Res. Pract. (2018), 2174957, https://doi.org/10.1155/2018/2174957, 2018.

[21] M.H. Chen, L.L. Wang, J.J. Chung, Y.H. Kim, P. Atluri, J.A. Burdick, Methods to assess shear-thinning hydrogels for application as injectable biomaterials, ACS Biomater. Sci. Eng. 3 (12) (2017) 3146–3160, https://doi.org/10.1021/acsbiomaterials.7b00734.

[22] S. Sant, S.L. Tao, O.Z. Fisher, Q. Xu, N.A. Peppas, A. Khademhosseini, Microfabrication technologies for oral drug delivery, Adv. Drug Deliv. Rev. 64 (6) (2012) 496–507, https://doi.org/10.1016/j.addr.2011.11.013.

[23] P. Kondiah, Y. Choonara, P. Kondiah, T. Marimuthu, P. Kumar, L.C. du Toit, et al., A review of injectable polymeric hydrogel systems for application in bone tissue engineering, Molecules 21 (11) (2016) 1580, https://doi.org/10.3390/molecules21111580.

[24] O. Catanzano, M.C. Straccia, A. Miro, F. Ungaro, I. Romano, G. Mazzarella, G. Santagata, F. Quaglia, P. Laurienzo, M. Malinconico, Spray-by-spray *in situ* cross-linking alginate hydrogels delivering a tea tree oil microemulsion, Eur. J. Pharmaceut. Sci. 66 (2015) 20–28, https://doi.org/10.1016/j.ejps.2014.09.018.

[25] Q. Xu, L.R. Guo, A. Sigen, Y.S. Gao, D.Z. Zhou, U. Greiser, C.F. Jack, H. Zhang, Y. X. Dong, C. Lara, F.G. Wang, W.G. Liu, W. Wang, W.X. Wang, Injectable hyperbranched poly(beta-amino ester) hydrogels with on-demand degradation profiles to match wound healing processes, Chem. Sci. 9 (8) (2018) 2179–2187, https://doi.org/10.1039/c7sc03913a.

[26] Y.P. Liang, X. Zhao, T.L. Hu, B.J. Chen, Z.H. Yin, P.X. Ma, B.L. Guo, Adhesive hemostatic conducting injectable composite hydrogels with sustained drug release and photothermal antibacterial activity to promote full-thickness skin regeneration during wound healing, Small 15 (12) (2019), e1900046, https://doi.org/10.1002/smll.201900046.

[27] R. Dimatteo, J.N. Darling, T. Segura, *In situ* forming injectable hydrogels for drug delivery and wound repair, Adv. Drug Deliv. Rev. 127 (2018) 167–184, https://doi.org/10.1016/j.addr.2018.03.007.

[28] N.Q. Tran, Y.K. Joung, E. Lih, K.D. Park, *In situ* forming and rutin-releasing chitosan hydrogels as injectable dressings for dermal wound healing, Biomacromol. 112 (2011) 2872–2880. https://doi.org/10.1021/bm200326g.

[29] H.Q. Tan, D.W. Jin, X. Qu, H. Liu, X. Chen, M. Yin, C.S. Liu, A peg-lysozyme hydrogel harvests multiple functions as a fit-to-shape tissue sealant for internal-use of body, Biomaterials 192 (2019) 392–404, https://doi.org/10.1016/j.biomaterials.2018.10.047.

[30] Y.P. Liang, X. Zhao, P.X. Ma, B.L. Guo, Y.P. Du, X.Z. Han, Ph-responsive injectable hydrogels with mucosal adhesiveness based on chitosan-grafted-dihydrocaffeic acid and oxidized pullulan for localized drug delivery, J. Colloid Interface Sci. 536 (2019) 224–234, https://doi.org/10.1016/j.jcis.2018.10.056.

[31] Y. Qin, Alginate fibres: an overview of the production processes and applications in wound management, Polym. Int. 57 (2) (2008) 171–180, https://doi.org/10.1002/pi.2296.

[32] J. Guan, Q.Y. Liu, J. Liu, Z.X. Cui, X. Zhang, S. Mao, Elucidation of alginate-drug miscibility on its crystal growth inhibition effect in supersaturated drug delivery

system, Carbohydr. Polym. 230 (2020), 115601, https://doi.org/10.1016/j.carbpol.2019.115601.
[33] I. Gholamali, M. Asnaashariisfahani, E. Alipour, Silver nanoparticles incorporated in ph-sensitive nanocomposite hydrogels based on carboxymethyl chitosan-poly (vinyl alcohol) for use in a drug delivery system, Regen. Eng. Transl. Med. 6 (2) (2019) 138–153, https://doi.org/10.1007/s40883-019-00120-7.
[34] A.M. Gholamali I, E. Alipour, S.A. Akhavan, In-situ synthesized carboxymethyl chitosan/poly(vinyl alcohol) bionanocomposite hydrogels containing nanoparticles with drugdelivery properties, Bull. Mater. Sci. 43 (2020) 264, https://doi.org/10.1007/s12034-020-02231-2.
[35] J. Wang, L. Wang, H. Yu, U.A. Zain, Y. Chen, Q. Chen, W.D. Zhou, H.T. Zhang, X. Chen, Recent progress on synthesis, property and application of modified chitosan: an overview, Int. J. Biol. Macromol. 88 (2016) 333–344, https://doi.org/10.1016/j.ijbiomac.2016.04.002.
[36] Y.S. Zhang, A. Khademhosseini, Advances in engineering hydrogels, Science 356 (2017) 6337, https://doi.org/10.1126/science.aaf3627.
[37] R. Hirose, N. Yoshida, Y. Naito, T. Yoshida, R. Bandou, T. Daidoji, K. Inoue, O. Dohi, H. Konishi, T. Nakaya, Y. Itoh, Development of sodium polyacrylate-based high-performance submucosal injection material with pseudoplastic fluid characteristics, ACS Biomater. Sci. Eng. 5 (12) (2019) 6794–6800, https://doi.org/10.1021/acsbiomaterials.9b01373.
[38] Y. Zhu, J.X. Xu, J. Cheng, Z. Zhang, B.Q. Zhu, T.Y. Chen, X.Y. Xu, Y. Wang, M. Y. Cai, P.H. Zhou, A novel injectable thermo-sensitive binary hydrogels system for facilitating endoscopic submucosal dissection procedure, United Eur. Gastroenterol. J. 7 (6) (2019) 782–789, https://doi.org/10.1177/2050640619825968.
[39] C.M. Hwang, S. Sant, M. Masaeli, N.N. Kachouie, B. Zamanian, S.H. Lee, A. Khademhosseini, Fabrication of three-dimensional porous cell-laden hydrogel for tissue engineering, Biofabrication 2 (3) (2010), 035003, https://doi.org/10.1088/1758-5082/2/3/035003.
[40] Q. Feng, J.K. Xu, K.Y. Zhang, H. Yao, N.Y. Zheng, L.Z. Zheng, J.L. Wang, K.C. Wei, X.F. Xiao, L. Qin, L.M. Bian, Dynamic and cell-infiltratable hydrogels as injectable carrier of therapeutic cells and drugs for treating challenging bone defects, ACS Cent. Sci. 5 (3) (2019) 440–450, https://doi.org/10.1021/acscentsci.8b00764.
[41] H. Hattori, H. Tsujimoto, K. Hase, M. Ishihara, Characterization of a water-soluble chitosan derivative and its potential for submucosal injection in endoscopic techniques, Carbohydr. Polym. 175 (2017) 592–600, https://doi.org/10.1016/j.carbpol.2017.08.028.
[42] C.Y. Cui, C.C. Fan, Y.H. Wu, M. Xiao, T.L. Wu, D.F. Zhang, X.Y. Chen, B. Liu, Z. Y. Xu, B. Qu, W.G. Liu, Water-triggered hyperbranched polymer universal adhesives: from strong underwater adhesion to rapid sealing hemostasis, Adv. Mater. 31 (49) (2019), e1905761, https://doi.org/10.1002/adma.201905761.
[43] Y. Wang, C.K. Adokoh, R. Narain, Recent development and biomedical applications of self-healing hydrogels, Expet Opin. Drug Deliv. 15 (1) (2018) 77–91, https://doi.org/10.1039/C7SC0 3913A.
[44] L. Liu, W. Yao, Y. Rao, X. Lu, J. Gao, Ph-responsive carriers for oral drug delivery: challenges and opportunities of current platforms, Drug Deliv. 24 (1) (2017) 569–581, https://doi.org/10.1080/10717544.2017.1279238.
[45] A.T. Hillel, S. Unterman, Z. Nahas, B. Reid, J.M. Coburn, J. Axelman, J.J. Chae, Q. Y. Guo, R. Trow, A. Thomas, Z.P. Hou, S. Lichtsteiner, D. Sutton, C. Matheson, P. Walker, N. David, S. Mori, J.M. Taube, J.H. Elisseeff, Photoactivated composite biomaterial for soft tissue restoration in rodents and in humans, Sci. Transl. Med. 13 (39) (2011), 93ra67, https://doi.org/10.1126/scitranslmed.3002331.
[46] J.G. Tidball, Regulation of muscle growth and regeneration by the immune system, Nat. Rev. Immunol. 17 (3) (2017) 165–178, https://doi.org/10.1038/nri.2016.150.
[47] A. Kumin, M. Schafer, N. Epp, P. Bugnon, C.B. Berclaz, A. Oxenius, A. Klippel, W. Bloch, S. Werner, Peroxiredoxin 6 is required for blood vessel integrity in wounded skin, J. Cell Biol. 179 (4) (2007) 747–760, https://doi.org/10.1083/jcb.200706090.
[48] C.C. Yates, P. Hebda, A. Wells, Skin wound healing and scarring: fetal wounds and regenerative restitution, Birth Def. Res. C Embryo Today 96 (4) (2012) 325–333, https://doi.org/10.1002/bdrc.21024.
[49] K. Chen, A. Vigliotti, M. Bacca, R.M. McMeeking, V.S. Deshpande, J.W. Holmes, Role of boundary conditions in determining cell alignment in response to stretch, Proc. Natl. Acad. Sci. U.S.A. 115 (5) (2018) 986–991, https://doi.org/10.1073/pnas.1715059115.
[50] G.M. Fomovsky, J.W. Holmes, Evolution of scar structure, mechanics, and ventricular function after myocardial infarction in the rat, Am. J. Physiol. Heart Circ. Physiol. 298 (1) (2010) H221–H228, https://doi.org/10.1152/ajpheart.00495.2009.
[51] L. Zhou, C. Dai, L. Fan, Y.H. Jiang, C. Liu, Z.G. Zhou, P.F. Guan, Y. Tian, J. Xing, X. J. Li, Y. Luo, P. Yu, C.Y. Ning, G.X. Tan, Injectable self-healing natural biopolymer-based hydrogel adhesive with thermoresponsive reversible adhesion for minimally invasive surgery, Adv. Funct. Mater. 31 (14) (2021), 2007457, https://doi.org/10.1002/adfm.202007457.